

A Control System For a Constrained Two-Body Wave Energy Converter

Shangyan Zou, Ossama Abdelkhalik

Abstract—Wave energy can be used to power oceanographic buoys. A new switching control strategy is developed in this paper for a two-body heaving wave energy converter that is composed of a floating cylinder and two rigidly connected submerged hemispheres. This control strategy is designed to prevent excessive displacement of the floating buoy that may occur due to the actuator force. This control strategy switches the control between a multi-resonant controller and a nonlinear damping controller, depending on the state of the system, to account for displacement constraints. This control strategy is developed using a one-degree-of-freedom dynamic model for the relative motion of the two bodies. Estimation of the relative motion, needed for feedback control, is carried out using a Kalman filter. Numerical simulations are conducted to select the proper mooring stiffness. The controller is tested with stochastic models of irregular waves in this paper. The performance of the controller with different sea states is discussed. Annual power production using this control strategy is presented based on real data in 2015 published by Martha's Vineyard Coastal Observatory.

Index Terms—Wave Energy Conversion, Two-Body Heaving Wave Energy Converter, Multi-Resonant Control, Kalman Filter, Annual Power Production

I. INTRODUCTION

Ocean waves contain abundant energy and it is considered to be reliable and have high power density [1]. The research on the hydrodynamics of a buoy interacting with a fixed structure (ex. seabed), or a moving reference started early seventies [2]–[4]. Wave energy converters can be categorized as: oscillating water column [5], overtopping converters [1], and point absorbers which are adopted in this paper.

Research on two-body systems (a buoy and a moving reference) received a great deal of interest over the past decades. Multiple designs of the two-body systems are available such as systems consisting of two concentric cylinders in which the outer cylinder is a hollow-shape [6], [7], and systems consisting of a float and a submerged buoy [8]. Since the shape of the submerged body has a significant impact on the performance of

the two body system [9], [10]. The shape of the proposed two body system in this paper is also carefully designed (shown in Fig. 1) which has demonstrated superiority on the relative radiation damping [11]. Further, though mooring system significantly impacts the power extraction of the two-body system [12] and the mooring force could be highly nonlinear for complex mooring system. The design of the mooring system is out of the scope of this paper, a simple catenary mooring which is represented as a linear spring [13] is adopted.

To optimize the performance of a two-body system, a proper control strategy is required. Although damping control provided a noticeable improvement on the energy harvesting of a two-body system [14] compared to single wave energy converter, the control is not capable to adjust the phase of system which loses optimality. The optimal Proportional-Derivative (PD) control of a two-body system can be designed by applying the Pontryagin Maximum Principle as proposed in reference [15]. Though optimal PD control introduces a significant improvement on energy conversion compared to single body system [16], the physical constraints are difficult to be implemented in the control design. In that context, the Pseudo-Spectrum control [17] and the Model Predictive control [18] developed for two-body systems handle the constraints without losing optimality. Reference [19] adopts the Model Predictive Control, and applies a one-body equivalent modelling approach that converts the two-degree-of-freedom model to a one-degree-of-freedom model.

The proposed control in this paper is the multi-resonant control [20] which is a time domain implementation of the complex conjugate control and is designed using the one-degree-of-freedom equivalent model. Regarding the physical constraints on the system, the control switches between the multi-resonant control and a nonlinear damping control [21]. The Kalman Filter is implemented to estimate the system response needed for control. Finally, to further validate the performance of the control in a constantly-changing wave climate, a full year power extraction is predicted. The proposed design is expected to supply the power need of the oceanographic application. The paper is organized as the followings: Section II introduces the dynamic model of the two-body heaving system. The control algorithm is presented in Section III, and the estimator is developed in Section IV. The simulation results are shown in Section V and further discussed in Section VI. Finally, the conclusion is drawn in Section VII.

Manuscript received 10 Oct 2019; revised 13 May; accepted 24 Aug; published 7 Sep, 2020. This is an open access article distributed under the terms of the Creative Commons Attribution 4.0 licence (CC BY <http://creativecommons.org/licenses/by/4.0/>). This article has been subject to single-blind peer review by a minimum of two reviewers. This work was supported in part by the National Science Foundation under Grant No. 1635362

Shangyan Zou was in the Department of Mechanical Engineering - Engineering Mechanics at Michigan Technological University, 1400 Townsend Dr, Houghton, MI, 49931 U.S.A. He is now in the Department of Aerospace Engineering at Iowa State University, 1200 Howe Hall, 537 Bissell Rd, Ames, IA, 50011 U.S.A (e-mail: shangyan@iastate.edu).

Ossama Abdelkhalik was in the Department of Mechanical Engineering - Engineering Mechanics at Michigan Technological University, 1400 Townsend Dr, Houghton, MI, 49931 U.S.A. He is now in the Department of Aerospace Engineering at Iowa State University, 1200 Howe Hall, 537 Bissell Rd, Ames, IA, 50011 U.S.A (e-mail: ossama@iastate.edu).

Digital Object Identifier <https://doi.org/10.36688/imej.2.51-61>

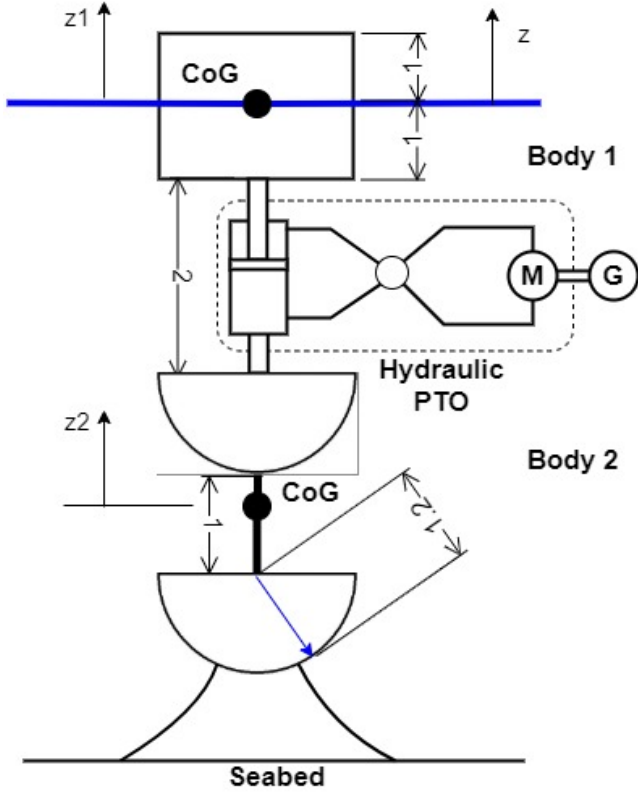


Fig. 1: The geometry of the two-body system.

II. THE DYNAMIC MODEL

The geometry of the two-body system adopted in this paper is shown in Fig. 1; it consists of a float (cylinder) and two hemispheres (submerged). The PTO is assumed installed between the two bodies, and the mooring system is connected to the lower mass. The first mass moves in vertical direction against the second mass which is moored to the seabed. The energy associated with the relative motion will be converted to electricity by applying hydraulic Power take-off (PTO) system. The PTO system is also assumed to be capable to supply the required reactive power. The model of the PTO system is not addressed in this paper. The application of the hydraulic system is inspired by [22], [23] which demonstrate a good energy conversion performance when it is applied to single point absorber. Motivated by the advantages of hydraulic system including its robustness, capacity for energy storage and speed control, the hydraulic PTO is also widely applied in two body systems [24]–[26]. In which, reference [25] presents the detailed modelling of hydraulic PTO which shows its superiority in power smoothing.

The center of gravity of the floating body is at $z = 0\text{m}$ which is 1m away from the bottom of the cylinder. The position z is measured from the mean water level (MWL). The center of gravity of the submerged body is at $z = -4.55\text{m}$. The dimensions of the device are summarized in Fig. 1 and the other information of the device are summarized in Table. I. In the table, $z_{1,max}$ and $z_{rel,max}$ denote the limitations for the motion of the first mass and the relative motion respectively. $u_{max,l}$ and $u_{max,h}$ denote the low and high control limit

TABLE I: The data applied in the simulation of the proposed device.

Symbol	Value	Unit
Device Properties		
m_{11}	4.637×10^3	kg
m_{22}	7.4192×10^3	kg
Physical Limitations		
$z_{1,max}$	1	m
$z_{rel,max}$	2	m
PTO Limitations		
$u_{max,l}$	7000	N
$u_{max,h}$	5×10^5	N
Mooring Stiffness		
K_m	3.63×10^6	N/m

subject to different wave conditions. K_m denotes the mooring stiffness and the value is applied in predicting annual power production.

Each of z_1 and z_2 is defined with respect to its original center of gravity. The equations of motion of the two-body system can be expressed as:

$$\begin{aligned}
 (m_{11} + m_{\infty,11})\ddot{z}_1 + m_{\infty,12}\ddot{z}_2 + B_{v1}\dot{z}_1 + h_{r,11} * \dot{z}_1 + \\
 h_{r,12} * \dot{z}_2 + K_1 z_1 = f_{e1} + u \\
 (m_{22} + m_{\infty,22})\ddot{z}_2 + m_{\infty,21}\ddot{z}_1 + B_{v2}\dot{z}_2 + h_{r,21} * \dot{z}_1 + \\
 h_{r,22} * \dot{z}_2 + K_m z_2 = f_{e2} - u
 \end{aligned} \quad (1)$$

where m_{11} and m_{22} are the rigid body masses of the two bodies. It is noted that in the current design the gravity of the second mass is balanced by the buoyancy force, thus the restoring force of the second mass in the dynamics is provided by the mooring system. The $m_{\infty,ij}$ is the added mass of i th body due to the j th mode, and $h_{r,ij}$ is the radiation impulse response function. They can be obtained from the commercial Boundary Element Software WAMIT [27]. The operator $*$ denotes the convolutional integral:

$$h_r * \dot{z} = \int_0^t h_r(t - \tau) \dot{z}(\tau) \delta\tau \quad (2)$$

The radiation damping coupling ($\vec{f}_{rad,d}$) between the two bodies can be extracted from Eq. (1) as:

$$\vec{f}_{rad,d} = \begin{bmatrix} h_{r,11} & h_{r,12} \\ h_{r,21} & h_{r,22} \end{bmatrix} * \begin{bmatrix} \dot{z}_1 \\ \dot{z}_2 \end{bmatrix} \quad (3)$$

which can be approximated by a state space model [28] as:

$$\begin{aligned}
 \dot{\vec{x}}_r &= A_r \vec{x}_r + B_r \begin{bmatrix} \dot{z}_1 \\ \dot{z}_2 \end{bmatrix} \\
 \vec{f}_{rad,d} &= C_r \vec{x}_r
 \end{aligned} \quad (4)$$

where \vec{x}_r represents the radiation states, and A_r , B_r and C_r can be identified from the radiation impulse response function. Further, The viscous damping coefficients of the two bodies are B_{v1} and B_{v2} respectively in Eq. (1). The K_1 is the hydro-static coefficient of the floating mass, and K_m is the mooring stiffness of the submerged mass. Additionally, the excitation forces of

the two bodies are f_{e1} and f_{e2} respectively which can be computed as:

$$\begin{aligned} f_{e1}(t) &= \sum_{n=1}^{N_w} \Re(\tilde{f}_{e1}(\omega_n)\eta(\omega_n)e^{i(-\omega_n t + \phi_n)}) \\ f_{e2}(t) &= \sum_{n=1}^{N_w} \Re(\tilde{f}_{e2}(\omega_n)\eta(\omega_n)e^{i(-\omega_n t + \phi_n)}) \end{aligned} \quad (5)$$

where $\tilde{f}_{e1}(\omega_n)$ and $\tilde{f}_{e2}(\omega_n)$ are the frequency dependent force coefficients which can also be obtained from WAMIT. The $\eta(\omega_n)$ is the frequency dependent wave elevation. ϕ_n is random phase shift and N_w is the number of frequencies of the excitation forces.

Let us define a state vector as $\vec{x} = [x_1, x_2, x_3, x_4, \vec{x}_r]^T$, where x_1 and x_2 are the displacements of the two bodies, x_3 and x_4 are the velocities of the two bodies. The equations of motion of the two-body system can then be written in a state space format as:

$$\dot{\vec{x}} = A\vec{x} + B\vec{f}_e + B\vec{u} \quad (6)$$

where:

$$\begin{aligned} A &= \begin{bmatrix} \begin{bmatrix} 0 & 0 \\ 0 & 0 \end{bmatrix} & \begin{bmatrix} 1 & 0 \\ 0 & 1 \end{bmatrix} & \begin{bmatrix} \vec{0} \\ \vec{0} \end{bmatrix} \\ -M^{-1}K & -M^{-1}B_v & -M^{-1}C_r \\ \vec{0} & \vec{0} & A_r \end{bmatrix} \\ B &= \begin{bmatrix} 0 & 0 \\ 0 & 0 \\ 1 & 0 \\ 0 & 1 \\ \vec{0} & \vec{0} \end{bmatrix} \end{aligned} \quad (7)$$

In addition, $\vec{f}_e = [f_{e1}, f_{e2}]^T$, $\vec{u} = [u, -u]^T$, and:

$$M = \begin{bmatrix} m_{11} + m_{\infty,11} & m_{\infty,12} \\ m_{\infty,21} & m_{22} + m_{\infty,22} \end{bmatrix} \quad (8)$$

$$K = \begin{bmatrix} K_1 & 0 \\ 0 & K_m \end{bmatrix} \quad (9)$$

$$B_v = \begin{bmatrix} B_{v1} & 0 \\ 0 & B_{v2} \end{bmatrix} \quad (10)$$

III. THE CONTROL ALGORITHM

A. The multi-resonant control

In this section, the multi-resonant control is derived for the two-body system by applying the one-body equivalent approach. Instead of deriving the control based on 2-degree-of-freedom equation of motion, the control can be derived based on the model that is expressed in terms of the relative motion. The optimal impedance of the control can be identified based on the equivalent intrinsic impedance. It is noted that, the one body equivalent approach can be applied in the proposed system since physically only one actuator is implemented between two bodies. The details of the derivation of one body equivalent approach can be

found in [19]. First, we need to consider the frequency domain expression of Eq. (1) as:

$$\begin{aligned} (m_1 + m_{a,11})(-i\omega)X_3 + (R_{11} + B_{v1})X_3 + \\ \frac{K_1}{-i\omega}X_3 + (R_{12} - i\omega m_{a,12})X_4 = F_{e1} + U \\ (m_2 + m_{a,22})(-i\omega)X_4 + (R_{22} + B_{v2})X_4 + \\ \frac{K_m}{-i\omega}X_4 + (R_{21} - i\omega m_{a,21})X_3 = F_{e2} - U \end{aligned} \quad (11)$$

where $m_{a,ij}$ and R_{ij} are the frequency dependent added mass and radiation damping respectively. X_3 and X_4 are the velocities of two bodies in frequency domain. F_{e1} , F_{e2} and U are the excitation forces and control expressed in frequency domain. It is noted that $R_{12} = R_{21}$ and $m_{a,12} = m_{a,21}$ [19]. Let us denote:

$$\begin{aligned} Z_{12} &= R_{12} - i\omega m_{a,12} \\ Z_{21} &= R_{21} - i\omega m_{a,21} \end{aligned} \quad (12)$$

We have $Z_{12} = Z_{21}$. For the convenience of mathematical derivation, the Z_{21} in the equations will later be replaced by Z_{12} . We can also define:

$$Z_1 = (m_1 + m_{a,11})(-i\omega) + \frac{K_1}{-i\omega} + R_{11} + B_{v1} \quad (13)$$

$$Z_2 = (m_2 + m_{a,22})(-i\omega) + \frac{K_m}{-i\omega} + R_{22} + B_{v2} \quad (14)$$

The form of the multi-resonant control of a monotonic wave is:

$$u = -K_p(x_1 - x_2) - K_d(x_3 - x_4) \quad (15)$$

where K_p and K_d are the proportional and derivative feedback gains respectively. This equation can also be expressed in frequency domain as:

$$U = -\left(\frac{K_p}{-i\omega} + K_d\right)(X_3 - X_4) \quad (16)$$

Hence, the impedance of the controller is $Z_c = \frac{iK_p}{\omega} + K_d$. Eq. (11) now can be expressed in a more condensed format as:

$$\begin{aligned} Z_1 X_3 + Z_{12} X_4 &= F_{e1} - Z_c(X_3 - X_4) \\ Z_{12} X_3 + Z_2 X_4 &= F_{e2} + Z_c(X_3 - X_4) \end{aligned} \quad (17)$$

It can be further written in a matrix format as:

$$\begin{bmatrix} Z_1 + Z_c & Z_{12} - Z_c \\ Z_{12} - Z_c & Z_2 + Z_c \end{bmatrix} \begin{bmatrix} X_3 \\ X_4 \end{bmatrix} = \begin{bmatrix} F_{e1} \\ F_{e2} \end{bmatrix} \quad (18)$$

The velocities can be solved as:

$$\begin{bmatrix} X_3 \\ X_4 \end{bmatrix} = \frac{1}{D} \begin{bmatrix} Z_2 + Z_c & -Z_{12} + Z_c \\ -Z_{12} + Z_c & Z_1 + Z_c \end{bmatrix} \begin{bmatrix} F_{e1} \\ F_{e2} \end{bmatrix} \quad (19)$$

where:

$$\begin{aligned} D &= (Z_1 + Z_c)(Z_2 + Z_c) - (Z_{12} - Z_c)^2 \\ &= Z_1 Z_2 - Z_{12}^2 + (Z_1 + Z_2 + 2Z_{12})Z_c \end{aligned} \quad (20)$$

As a result, the relative motion can be obtained:

$$\begin{aligned} X_{rel} &= X_3 - X_4 \\ &= \frac{1}{D} ((Z_2 + Z_c)F_{e1} - (Z_1 + Z_c)F_{e2} + \\ &\quad (Z_c - Z_{12})(F_{e2} - F_{e1})) \\ &= \frac{1}{D} ((Z_2 + Z_{12})F_{e1} - (Z_1 + Z_{12})F_{e2}) \end{aligned} \quad (21)$$

If we denote $Z_0 = Z_1 + Z_2 + 2Z_{12}$, we will have:

$$D = Z_1 Z_2 - Z_{12}^2 + Z_0 Z_c \quad (22)$$

The equivalent excitation force can be modelled as [19]:

$$F_{eq} = \frac{(Z_2 + Z_{12})F_{e1} - (Z_1 + Z_{12})F_{e2}}{Z_0} \quad (23)$$

Substitute Eq. (22) and (23) into Eq. (21) we get:

$$X_{rel} = \frac{F_{eq} Z_0}{Z_1 Z_2 - Z_{12}^2 + Z_0 Z_c} = \frac{F_{eq}}{\frac{Z_1 Z_2 - Z_{12}^2}{Z_0} + Z_c} \quad (24)$$

If we define the equivalent intrinsic impedance $Z_{i,eq}$ as:

$$Z_{i,eq} = \frac{Z_1 Z_2 - Z_{12}^2}{Z_0} \quad (25)$$

Then Eq. (24) becomes:

$$X_{rel} = \frac{F_{eq}}{Z_{i,eq} + Z_c} \quad (26)$$

The 2-degree-of-freedom equation of motion finally is transformed to a single degree of freedom equation based on relative motion. The optimal impedance of the controller should be designed to be the complex conjugate of the equivalent intrinsic impedance [18], [19], [29]:

$$Z_c = Z_{i,eq}^* \quad (27)$$

Since $Z_{i,eq} = \Re(Z_{i,eq}) + i\Im(Z_{i,eq})$, We have:

$$Z_c = Z_{i,eq}^* = \Re(Z_{i,eq}) - i\Im(Z_{i,eq}) \quad (28)$$

The PD feedback gain can be computed as:

$$K_p = -\Im(Z_{i,eq})\omega \quad (29)$$

$$K_d = \Re(Z_{i,eq}) \quad (30)$$

The derivation of optimal feedback gains K_p and K_d with a monotonic wave is extendable to the irregular wave condition. The multi-resonant control under the irregular wave condition takes the form of:

$$\begin{aligned} u &= \sum_{n=1}^N u_n \\ &= \sum_{n=1}^N -K_{p,n}(x_{1,n} - x_{2,n}) - K_{d,n}(x_{3,n} - x_{4,n}) \end{aligned} \quad (31)$$

where the n^{th} component of the displacements, $x_{1,n}$ and $x_{2,n}$, response to the dynamics of the n^{th} system:

$$\begin{bmatrix} \ddot{x}_{1,n} \\ \ddot{x}_{2,n} \end{bmatrix} = M_a^{-1}(\vec{F}_e + \vec{u} - (B_v + R) \begin{bmatrix} x_{3,n} \\ x_{4,n} \end{bmatrix} - K \begin{bmatrix} x_{1,n} \\ x_{2,n} \end{bmatrix}) \quad (32)$$

where

$$M_a = \begin{bmatrix} m_{11} + m_{a,11} & m_{a,12} \\ m_{a,21} & m_{22} + m_{a,22} \end{bmatrix} \quad (33)$$

$$R = \begin{bmatrix} R_{11} & R_{12} \\ R_{21} & R_{22} \end{bmatrix} \quad (34)$$

In Eq. (31), the $x_{3,n}$ and $x_{4,n}$ are the n^{th} components of velocities of the two bodies. So the n^{th} PD control

gains can be computed from the equivalent intrinsic impedance of the n^{th} system as:

$$K_{p,n} = -\Im(Z_{i,eq,n})\omega_n \quad (35)$$

$$K_{d,n} = \Re(Z_{i,eq,n}) \quad (36)$$

The number of feedback components of the multi-resonance control (N) is a design variable.

B. The switching control

To account for the physical limitations on the two-body system, a switching control strategy is proposed. The control will switch between two control laws where one is the multi-resonant control and the other one is the nonlinear damping control. A switching criteria x_{sc} is defined based on the relative displacement of the two bodies. The algorithm of this control law is summarized below:

```

if  $\|x_{rel}\| < x_{sc}$  then
  if  $\|u_{opt}\| < \gamma$  then
     $u_{opt} = \sum_{n=1}^N -K_{p,n}(x_{1,n} - x_{2,n}) - K_{d,n}(x_{3,n} - x_{4,n})$ 
  else
     $u_{opt} = \text{sign}(u_{opt})\gamma$ 
  end if
else
  if  $\|u_{opt}\| < \gamma$  then
     $u_{opt} = -\alpha(c_0 + c_1\|x_{rel}\| + c_2\|x_{rel}\|^2 + c_3\|x_{rel}\|^3)\dot{x}_{rel}$ 
  else
     $u_{opt} = \text{sign}(u_{opt})\gamma$ 
  end if
end if

```

where $x_{rel} = x_1 - x_2$ is the relative displacement, γ is the limitation of the control force. The parameters α , c_0 , c_1 , c_2 and c_3 are the nonlinear damping control coefficient. The nonlinear damping control requires the information of the relative motion, therefore the measurements of relative motion will be fed into the control.

IV. THE ESTIMATOR

Since the multi-resonance control requires the information of the n^{th} components of the system responses, the Kalman Filter is implemented for estimating system response components. The displacements of the two bodies can be approximated as:

$$\begin{aligned} x_1 &= \sum_{n=1}^N x_{1,n} \approx \sum_{n=1}^N a_{1,n} \cos(\omega_{0,n}t) + b_{1,n} \sin(\omega_{0,n}t) \\ x_2 &= \sum_{n=1}^N x_{2,n} \approx \sum_{n=1}^N a_{2,n} \cos(\omega_{0,n}t) + b_{2,n} \sin(\omega_{0,n}t) \end{aligned} \quad (37)$$

where $\omega_{0,n}$ is the n^{th} component of the vector $\vec{\omega}_0$ which has the components evenly distributed in a certain range. The $a_{1,n}$, $b_{1,n}$, $a_{2,n}$ and $b_{2,n}$ are the n^{th} components of the vectors \vec{a}_1 , \vec{b}_1 , \vec{a}_2 and \vec{b}_2 which are the coefficients of the Fourier terms. Let the estimated

states $\hat{\vec{X}} = [\hat{a}_1, \hat{b}_1, \hat{a}_2, \hat{b}_2]^T$, the dynamics of the Kalman Filter is:

$$\dot{\hat{\vec{X}}} = \vec{0} \quad (38)$$

$$\dot{P} = GQG^T \quad (39)$$

where P is the error covariance matrix, G is the weight of the process noise, Q is the process noise covariance matrix. The measurement model of the Kalman Filter can be constructed as:

$$\tilde{y}_k = \begin{bmatrix} \tilde{z}_1 \\ \tilde{z}_2 \end{bmatrix} = H_k \hat{\vec{X}}_k + \vec{v}(t) \quad (40)$$

where $\vec{v}(t)$ is the measurement noise vector and:

$$H_k = \begin{bmatrix} \cos(\vec{\omega}_0 t) & \sin(\vec{\omega}_0 t) & \vec{0} & \vec{0} \\ \vec{0} & \vec{0} & \cos(\vec{\omega}_0 t) & \sin(\vec{\omega}_0 t) \end{bmatrix} \quad (41)$$

To update the estimation at each stage we collect the measurements, the Kalman Gain needs to be computed as:

$$K_k = P_k^- H_k^T [H_k P_k^- H_k^T + R_k]^{-1} \quad (42)$$

where R_k is the measurement noise covariance matrix at k^{th} stage. Finally, the process of the continuous-discrete Kalman Filter is summarized below:

- (1). Propagate Eq. (38) and (39) to next stage k , to obtain $\hat{\vec{X}}_k^-$ and P_k^- .
- (2). Compute the Kalman Gain using Eq. (42).
- (3). Update the state estimation $\hat{\vec{X}}_k^-$ and error covariance matrix P_k^- using equations below:

$$\begin{aligned} \hat{\vec{X}}_k^+ &= \hat{\vec{X}}_k^- + K_k [\tilde{y}_k - H_k \hat{\vec{X}}_k^-] \\ P_k^+ &= [I - K_k H_k] P_k^- \end{aligned} \quad (43)$$

- (4). Obtain the updated state estimation and error covariance matrix: $\hat{\vec{X}}_k^+$ and P_k^+ .
- (5). Repeat step (1).

The initial guess of state estimation $\hat{\vec{X}}_0$ and error covariance matrix P_0 is required to start the Kalman Filter. In this paper, the Kalman Filter is initialized with the available hydrodynamic coefficients as:

$$\hat{\vec{X}}_0 = [\hat{a}_{1,0}, \hat{b}_{1,0}, \hat{a}_{2,0}, \hat{b}_{2,0}]^T \quad (44)$$

$$P_0 = 5 \frac{\hat{\vec{X}}_0 \hat{\vec{X}}_0^T}{2} \quad (45)$$

where the n^{th} component of $\hat{\vec{X}}_0$ is computed as:

$$\begin{aligned} \hat{a}_{1,n,0} &= \Re(Z_n(1)) \\ \hat{b}_{1,n,0} &= \Im(Z_n(1)) \\ \hat{a}_{2,n,0} &= \Re(Z_n(2)) \\ \hat{b}_{2,n,0} &= \Im(Z_n(2)) \end{aligned} \quad (46)$$

and:

$$\begin{aligned} V_n &= \begin{bmatrix} Z_{1,n} + Z_{c,n} & Z_{12,n} - Z_{c,n} \\ Z_{21,n} - Z_{c,n} & Z_{2,n} + Z_{c,n} \end{bmatrix}^{-1} \begin{bmatrix} F_{e1}(\omega_n) \frac{\eta_{m,ax}}{N} \\ F_{e2}(\omega_n) \frac{\eta_{m,ax}}{N} \end{bmatrix} \\ Z_n &= \frac{V_n}{-i\omega_n} \end{aligned} \quad (47)$$

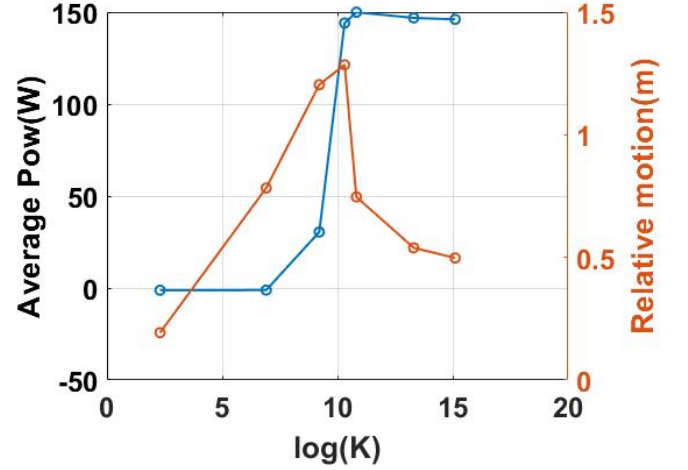


Fig. 2: The power extraction and the relative motion with different mooring stiffness K .

V. SIMULATION RESULTS

The simulation results are presented in this section. In the simulated system, the mass of the floating body in Fig. 1 is $4.637 \times 10^3 \text{kg}$ and the mass of the submerged body is $7.4192 \times 10^3 \text{kg}$. All the numerical results are simulated in Matlab[®].

A. The Multi-Resonant control with different mooring stiffness

In this paper, a simple catenary mooring is adopted [13] which is represented as a spring ($K_m z_2$). It is critical to have a proper design of the mooring stiffness K_m . As a result, the energy production of the two-body system by applying multi-resonant control with different mooring stiffness is examined first. These mooring stiffness are: $[10, 1000, 1 \times 10^4, 3 \times 10^4, 5 \times 10^4, 6 \times 10^5, 3.63 \times 10^6] \text{N/m}$. The wave applied in the simulations has a Bretschneider wave spectrum with a significant height (H_s) of 0.3m and a peak period (T_p) of 9s. A relative small wave condition is applied since the multi-resonant control does not consider the physical constraints. Moreover, the maximum control effort is 7000N which is affordable by a hydraulic PTO unit. Fig. 2 shows the power extraction and maximum relative motion versus different mooring stiffness. As indicated in the figure, the power extraction of the two-body system is stable around 150W when the mooring stiffness is greater than $3 \times 10^4 \text{N/m}$. However, the maximum relative motion shows a decreasing trend when the mooring stiffness is increasing from $3 \times 10^4 \text{N/m}$ to $3.63 \times 10^6 \text{N/m}$. Further, Fig. 3 shows the power extracted from the two-body heaving systems by applying one body equivalent approach and two-body approach. Clearly, by applying the one body equivalent approach, the energy production is not only higher, but also more stable when the mooring stiffness is greater than $3 \times 10^4 \text{N/m}$.

B. The performance of the Multi-Resonant Control

In this section, the details of the performance of the multi-resonant control are presented. The wave applied

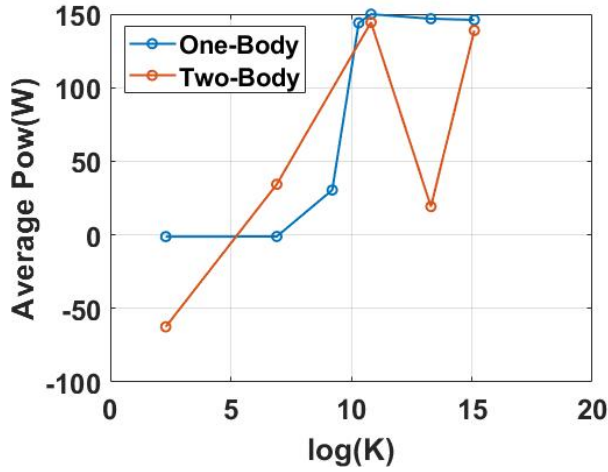


Fig. 3: The comparison between the power extracted by applying the one body approach and two body approach with different mooring stiffness K .

in the simulation has a Bretschneider wave spectrum with a significant height of 0.3m and a peak period of 9s. Based on the discussion in last section, the mooring stiffness is selected as $5 \times 10^4 \text{N/m}$ since the energy production is the maximum under this mooring stiffness. Additionally, by selecting this mooring stiffness, the expenditures on the mooring system can be significantly saved compared to choosing a very high mooring stiffness. Furthermore, the multi-resonant control contains 4 PD feedback controls in response to the frequencies $\vec{\omega} = [0.005, 0.465, 0.925, 1.385] \text{rad.s}^{-1}$ and its limitation is 7000N. The limitations of the absolute motion of the first mass is 1m and of the relative motion $\|x_1 - x_2\|$ is 2m to prevent collision between two bodies. The power production profiles of the two bodies are shown in Fig. 4, and the total average power of the two bodies is 149.92W. As shown in the figure, significant reactive power is required since the multi-resonant control focuses on optimizing the energy production. Fig. 5 shows the energy extraction of the two bodies. As indicated in the figure, the energy harvested by the first body is $1.173 \times 10^5 \text{J}$ and by the second body is $2.707 \times 10^4 \text{J}$. Moreover, the displacement of the two bodies are presented in Fig. 6 and Fig. 7 respectively. The estimations of the displacement show a good agreement with the true signals and the maximum absolute motions of the two bodies are both smaller than 0.5m. The relative motion between two bodies is shown in Fig. 8, and its maximum magnitude is around 0.85m. Fig. 9 shows the motion of the two bodies measured from the mean water level to the center of gravity of the two bodies.

C. The performance of the switching control

Though the multi-resonant control shows promising performance on controlling the two-body system, the physical limitations are not considered in the control. The wave applied in the simulation shown in last section is small which naturally guarantees the motions of the two bodies are within feasible range. However, most of the ocean wave conditions are stronger and

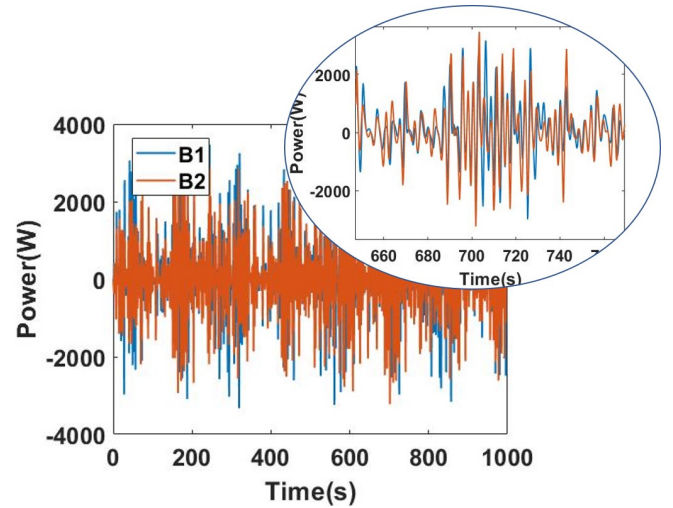


Fig. 4: The power extracted from the first and the second mass with control limitation 7000N and mooring stiffness $5 \times 10^4 \text{N/m}$.

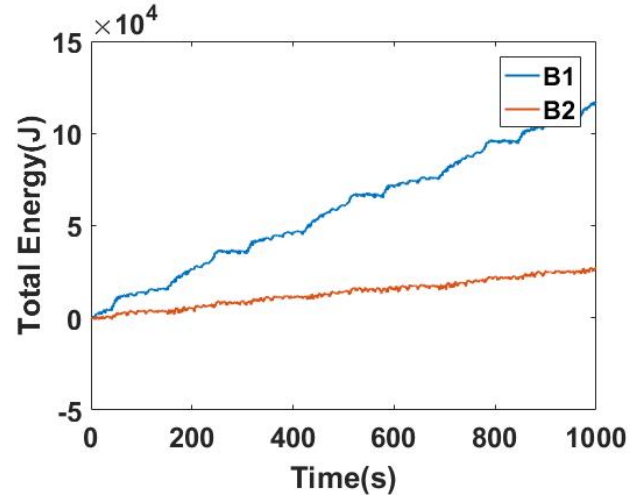


Fig. 5: The energy extracted from the first and the second mass with control limitation 7000N and mooring stiffness $5 \times 10^4 \text{N/m}$.

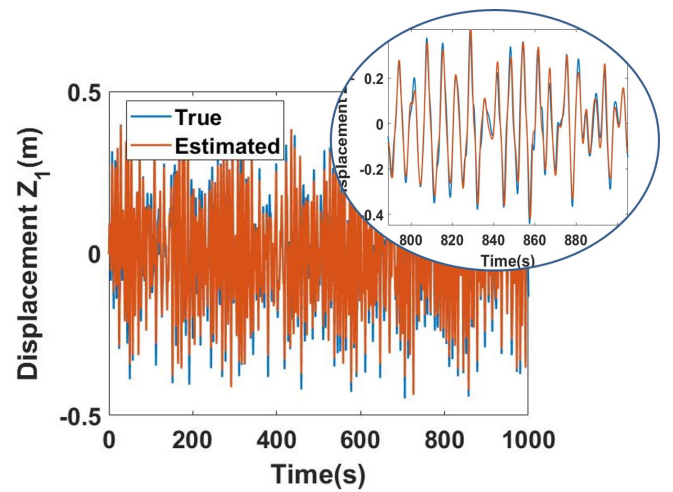


Fig. 6: The estimation of the displacement (z_1) of the first mass.

contain more energy. Therefore, a switching control is proposed and numerically examined in this section. The mooring stiffness is selected to be $3.63 \times 10^6 \text{N/m}$

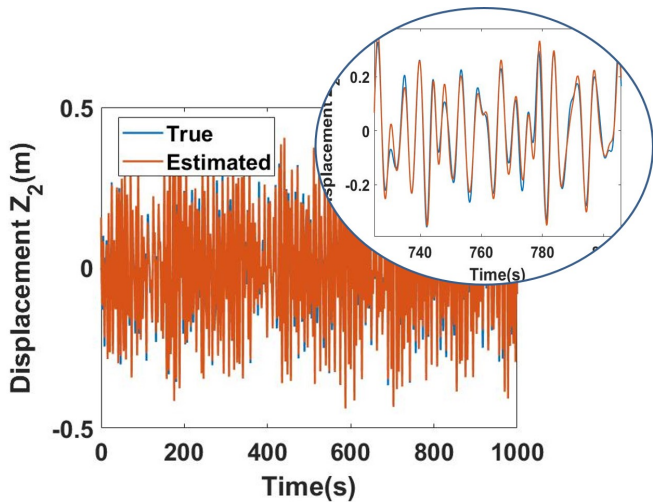


Fig. 7: The estimation of the displacement (z_2) of the second mass.

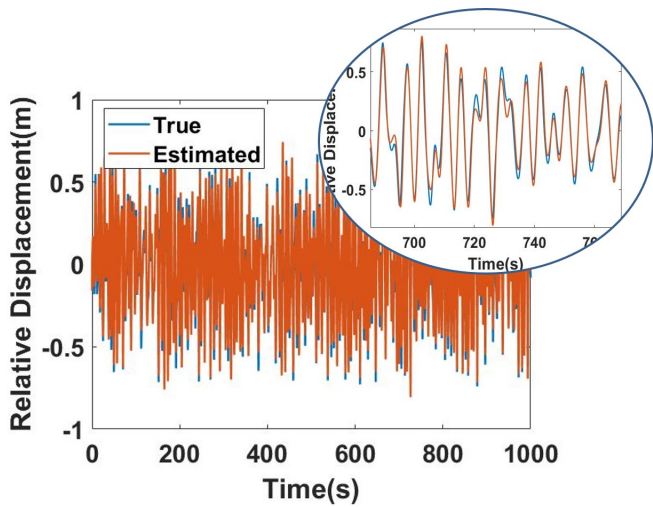


Fig. 8: The estimation of the relative displacement ($z_1 - z_2$).

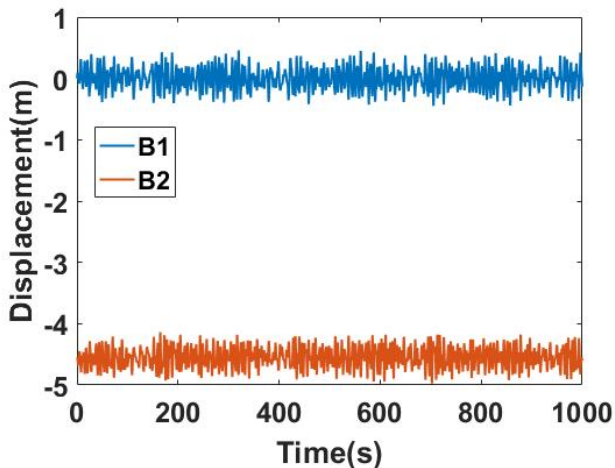


Fig. 9: The displacement of the first and the second mass measured from the mean water level to the center of gravity of the two bodies.

to keep the two-body system survival in extreme wave conditions. The sea states applied in the simulations are extracted from the one-year observation data which is recorded by Marthas Vineyard Coastal Observatory (MVCO) (<http://www.whoi.edu/mvco>)

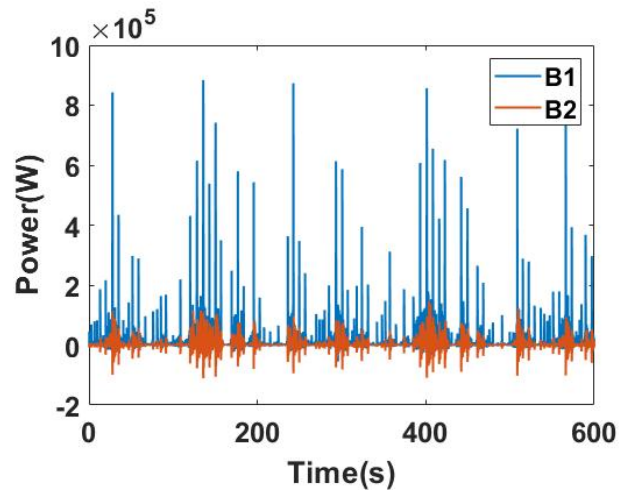


Fig. 10: The power extracted by applying switching control with control limitation 5×10^5 N under the wave condition $H_s = 3.8$ m and $T_p = 16$ s.

[30]. Since most of the ocean wave fields are dominated by swell waves [31], the waves generated by the wind will not be included in the simulations. The significant wave heights of the sea conditions vary from 0.1m to 3.8m and the peak periods vary from 7s to 16s. For even larger waves in more energetic sites, the proposed design is expected to be more dominated by nonlinear damping control and the system is expected to operate in survival mode under extreme waves. The numerical simulation is first conducted on validating the performance of the switching control under an extreme wave condition in the current site ($H_s = 3.8$ m and $T_p = 7$ s). As shown in Fig. 11, the absolute motion of the first mass (profile in blue) is beyond the limitation when the maximum control effort is only 7000N. Accordingly, more control effort is required to constrain the motion of the system. As presented in the same figure, the absolute displacement of the first body (profile in red) is within the feasible range when the maximum control effort is 5×10^5 N. It is noted that the switching criteria is $x_{sc} = 0.1$ m when higher control limitation is applied, compared to $x_{sc} = 0$ m when lower control limitation is applied. This indicates, although, the nonlinear damping control is dominant to keep the system survive from extreme wave conditions, there is room for multi-resonant control when more control effort is allowed.

The performance of the switching control in terms of energy extraction under a variety of wave conditions is shown in Fig. 12 and 13 respectively. In which, the control limitations are assumed to be 7000N and 5×10^5 N respectively since the wave conditions applied in Fig. 13 are stronger than the waves in Fig. 12. The power extraction during the extreme wave condition ($H_s = 3.8$ m and $T_p = 16$ s) is presented in Fig. 10. From the figure, we can tell the reactive power is mitigated when the nonlinear damping control is applied to constrain the motion (compare to Fig. 4). In addition, the maximum power extracted from strong waves with high control limitation is 1.2×10^4 W compared to 2000W extracted from small waves with low control limitation. Further, these two figures show a simi-

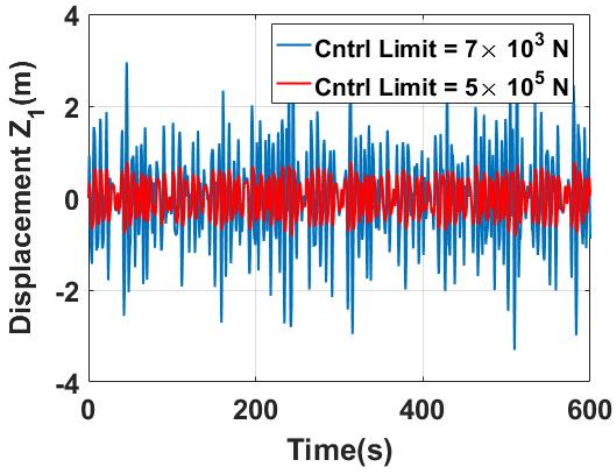


Fig. 11: The displacement of the first mass with a low control limitation and a high control limitation.

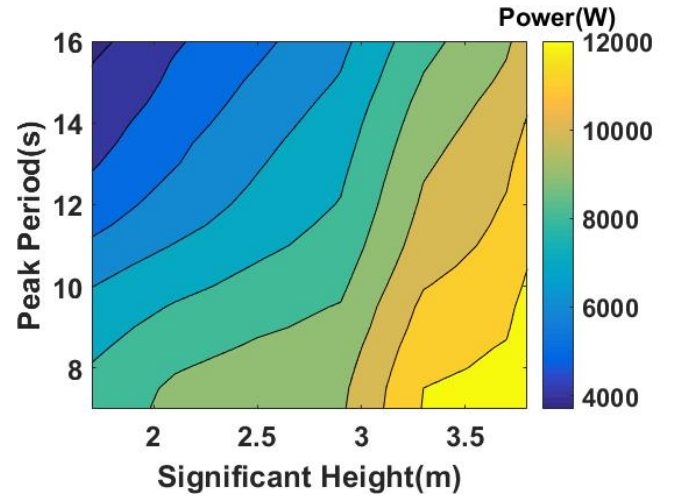


Fig. 13: The power extraction of different waves with a high control limitation.

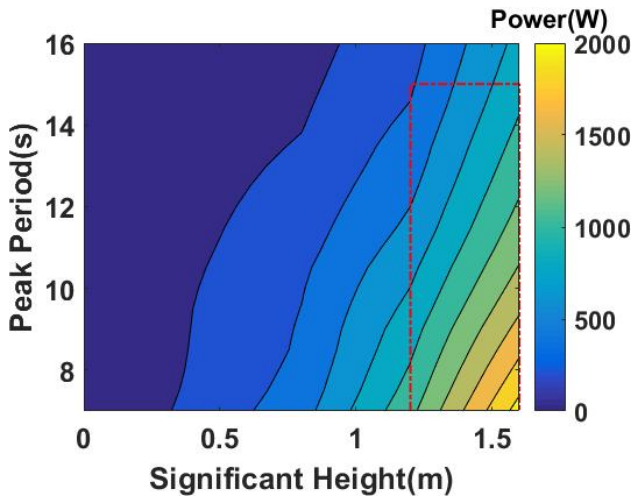


Fig. 12: The power extraction of different waves with a low control limitation.

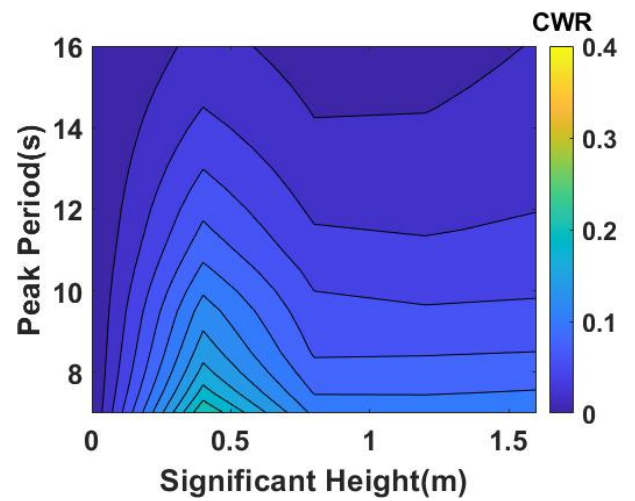


Fig. 14: The CWR of the proposed control with a low control limitation.

lar trend for the energy production versus significant height and peak period. Approximately, by applying switching control, more energy can be harvested from the wave that has higher significant height and lower peak period. The highlighted region in Fig. 12 represents a small violation of the motion constraint ($\leq \pm 0.2\text{m}$) due to limited control effort. However, the data will still be kept for the convenience of predicting annual power production later.

The Capture Width Ratio (CWR) [32] of the proposed control are presented in Fig. 14 and Fig. 15. As shown in the figures the maximum CWR is around 0.4 when the wave condition is around $H_s = 1.7\text{m}$ and $T_p = 7\text{s}$. The CWR decreases under large waves when the wave becomes more energetic since the nonlinear damping control will be more dominant to constrain the motion of the device. The CWR also decreases under small waves ($H_s < 0.5\text{m}$) when the wave contains less energy, since the multi-resonant control is more dominant which focuses on maximizing the energy production.

VI. DISCUSSION

The proposed multi-resonant control by applying the one body equivalent approach can produce consider-

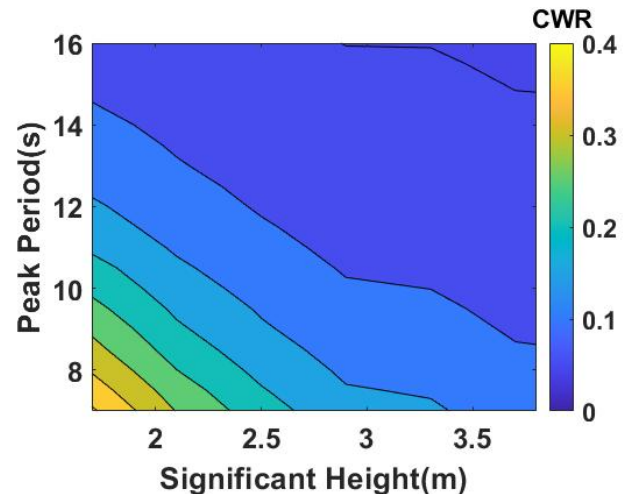


Fig. 15: The CWR of the proposed control with a high control limitation.

able energy with a proper selection of the mooring stiffness. To consider the physical limitations, this control is further improved by applying the switching control strategy. By applying this strategy, the two-body system is able to survive under extreme wave

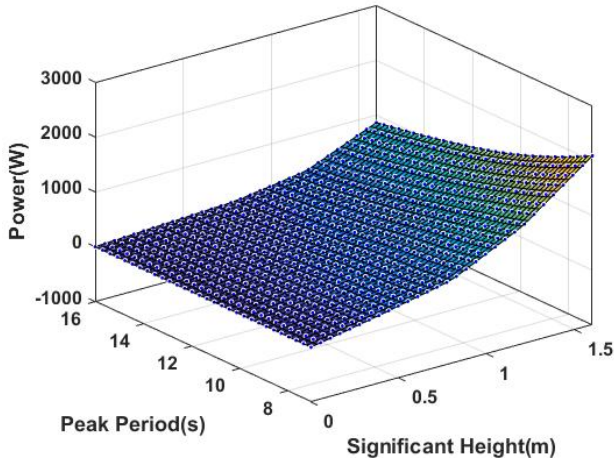


Fig. 16: The fitted power extraction of different waves with a low control limitation.

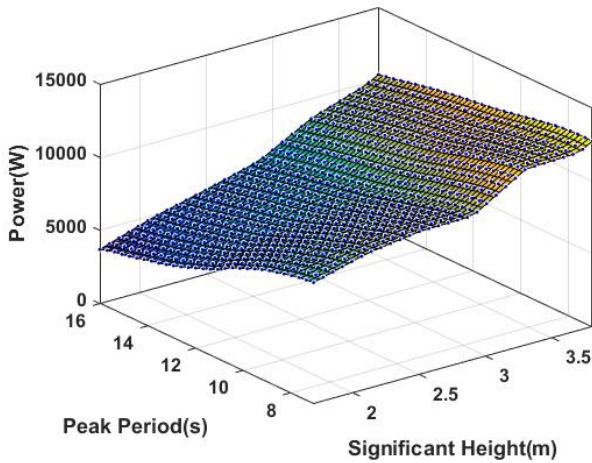


Fig. 17: The fitted power extraction of different waves with a high control limitation.

conditions. Although, the superiority of the proposed control is numerically demonstrated in previous case studies, we would like to further validate the performance of the switching control by predicting the annual power production of the two-body system. The dynamics that describe the interaction between the two-body system and the wave is linear which is not accurate when two-body system is under strong waves. However, this paper focuses on introducing the control, and the investigation of different dynamics for the two-body system under different wave conditions is beyond the scope of this paper. Therefore, for the sake of presenting the control performance, the linear model is applied for all the wave conditions.

To predict the energy harvesting over a year and save the computational cost, the energy extractions under different wave conditions are approximated by a function f :

$$P \approx f(H_s, T_p) \quad (48)$$

The fitted power production surfaces are shown in Fig. 16 and 17 respectively. In which, Fig. 16 applies low control limitation and Fig. 17 applies high control limitation. The linear interpolation method is applied

to generate the function f . The annual power harvesting is then predicted by applying function f and different wave conditions over a year. Fig. 18 shows the annual power production of 2015, in which the red region denotes the power produced with a high control limitation and the green region denotes the power produced with a low control limitation. As indicated in the figure, the mean power production of the two-body system is 626.8159W in 2015. Moreover, if we assume the two-body system is under survival mode (no power production) when the significant heights of the waves are greater than 1.6m, the mean power extraction is 308.9641W. This power is around 50% of the power production when there is no survival mode allowed, although there are only 14 days in a year when the two-body system interacts with extreme waves.

VII. CONCLUSION

This paper investigated the application of wave power to supply the power needs of oceanographic buoys. A multi-resonant control is designed for the two-body system proposed in this paper by applying the one body equivalent approach. To consider the physical limitations, the switching control is introduced. A Kalman Filter is implemented to estimate the states at current time. The numerical simulation results show that the energy extraction of the switching control is considerable with proper selection of the mooring stiffness and control limitation. Further, the control is tested in different wave conditions. The simulated energy productions are utilized to predict the annual power extraction. The predicted average power is 626.8159W which can be applied to support the energy demand of oceanographic buoys in the future.

ACKNOWLEDGEMENT

This material is based upon work supported by the National Science Foundation under Grant Number 1635362. Dr. Umesh Korde suggested the use of the one body dynamic model presented in reference [19].

REFERENCES

- [1] B. Drew, A. R. Plummer, and M. N. Sahinkaya, "A review of wave energy converter technology," *Proceedings of the Institution of Mechanical Engineers, Part A: Journal of Power and Energy*, vol. 223, no. 8, pp. 887–902, 2009. [Online]. Available: <http://pia.sagepub.com/content/223/8/887.abstract>
- [2] J.N.Newman, "The interaction of stationary vessels with regular waves," in *Proceeding 11th symposium, Naval hydrodynamics*, London, 1976. [Online]. Available: http://journals.cambridge.org/article_S0022112076001109
- [3] C. C. Mei, "Power extraction from water waves," *Journal of Ship Research*, vol. 20, pp. 63–66, June 1976.
- [4] K. Budal, "Theory for absorption of wave power by a system of interacting bodies," *Journal of Ship Research*, vol. 21, pp. 248–253, 1977.
- [5] A. F. Falcão and J. C. Henriques, "Oscillating-water-column wave energy converters and air turbines: A review," *Renewable Energy*, vol. 85, pp. 1391–1424, 2016.
- [6] C. Cochet and R. W. Yeung, "Two-component axisymmetric wave-energy absorber-analysis of dynamics and geometric proportions," in *The 27th International Workshop on Water Waves and Floating Bodies, Copenhagen, Denmark*. Citeseer, 2012.

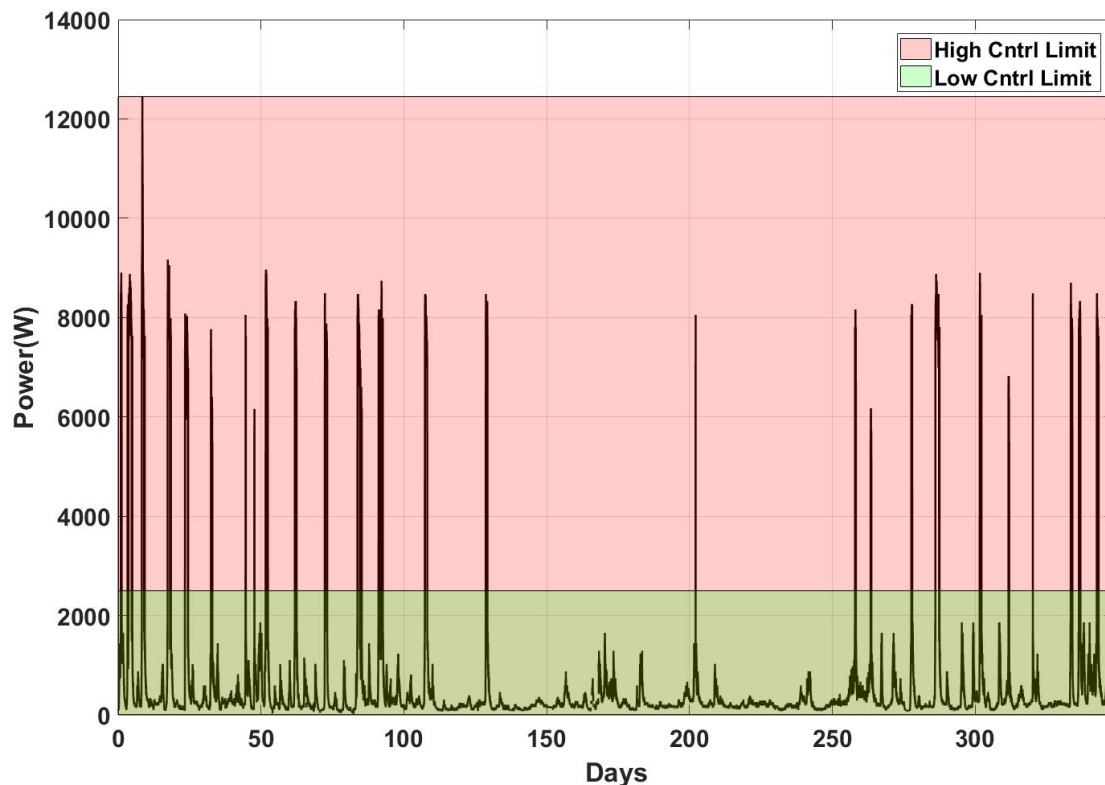


Fig. 18: The predicted power extraction of one year.

- [7] J. R. Kim, Y. H. Bae, I. H. Cho *et al.*, "Relative heave motion responses of a floating dual-buoy wave energy converter in waves," in *The Twenty-fifth International Ocean and Polar Engineering Conference*. International Society of Offshore and Polar Engineers, 2015.
- [8] Y.-H. Yu and Y. Li, "Reynolds-averaged navier-stokes simulation of the heave performance of a two-body floating-point absorber wave energy system," *Computers & Fluids*, vol. 73, pp. 104–114, 2013.
- [9] E. Al Shami, X. Wang, R. Zhang, and L. Zuo, "A parameter study and optimization of two body wave energy converters," *Renewable energy*, vol. 131, pp. 1–13, 2019.
- [10] D. Son, V. Belissen, and R. W. Yeung, "Performance validation and optimization of a dual coaxial-cylinder ocean-wave energy extractor," *Renewable Energy*, vol. 92, pp. 192–201, 2016.
- [11] U. A. Korde, J. Song, R. D. Robinett, and O. O. Abdelkhalik, "Hydrodynamic considerations in near-optimal control of a small wave energy converter for ocean measurement applications," *Marine Technology Society Journal*, vol. 51, no. 6, pp. 44–57, 2017.
- [12] M. J. Muliawan, Z. Gao, T. Moan, and A. Babarit, "Analysis of a two-body floating wave energy converter with particular focus on the effects of power take-off and mooring systems on energy capture," *Journal of Offshore Mechanics and Arctic Engineering*, vol. 135, no. 3, p. 031902, 2013.
- [13] B. Bosma, T. K. Brekken, H. T. Özkan-Haller, and S. C. Yim, "Wave energy converter modeling in the time domain: A design guide," in *2013 1st IEEE Conference on Technologies for Sustainability (SusTech)*. IEEE, 2013, pp. 103–108.
- [14] J. Engström, M. Eriksson, J. Isberg, and M. Leijon, "Wave energy converter with enhanced amplitude response at frequencies coinciding with swedish west coast sea states by use of a supplementary submerged body," *Journal of Applied Physics*, vol. 106, no. 6, p. 064512, 2009.
- [15] J. J. Cândido and P. A. Justino, "Modelling, control and pontryagin maximum principle for a two-body wave energy device," *Renewable Energy*, vol. 36, no. 5, pp. 1545–1557, 2011.
- [16] C. Liang and L. Zuo, "On the dynamics and design of a two-body wave energy converter," *Renewable Energy*, vol. 101, pp. 265–274, 2017.
- [17] G. Bacelli, J. V. Ringwood, and J.-C. Gilloteaux, "A control system for a self-reacting point absorber wave energy converter subject to constraints," *IFAC Proceedings Volumes*, vol. 44, no. 1, pp. 11 387–11 392, 2011.
- [18] S. Olaya, J.-M. Bourgeot, and M. Benbouzid, "Optimal control for a self-reacting point absorber: A one-body equivalent model approach," in *Power Electronics and Application Conference and Exposition (PEAC), 2014 International*. IEEE, 2014, pp. 332–337.
- [19] J. Falnes, "Wave-energy conversion through relative motion between two single-mode oscillating bodies," *Journal of Offshore Mechanics and Arctic Engineering*, vol. 121, no. 1, pp. 32–38, 1999.
- [20] O. Abdelkhalik, S. Zou, R. D. Robinett, G. Bacelli, D. G. Wilson, R. Coe, and U. Korde, "Multiresonant feedback control of a three-degree-of-freedom wave energy converter," *IEEE Transactions on Sustainable Energy*, vol. 8, no. 4, pp. 1518–1527, 2017.
- [21] S. Zou, O. Abdelkhalik, U. Korde, and R. Robinett, "Switching control for constrained wave energy converters," in *OCEANS 2017-Anchorage*. IEEE, 2017, pp. 1–7.
- [22] F. d. O. António, "Modelling and control of oscillating-body wave energy converters with hydraulic power take-off and gas accumulator," *Ocean engineering*, vol. 34, no. 14-15, pp. 2021–2032, 2007.
- [23] S. Zou and O. Abdelkhalik, "Control of wave energy converters with discrete displacement hydraulic power take-off units," *Journal of Marine Science and Engineering*, vol. 6, no. 2, p. 31, 2018.
- [24] E. Anderlini, D. Forehand, E. Bannon, Q. Xiao, and M. Abusara, "Reactive control of a two-body point absorber using reinforcement learning," *Ocean Engineering*, vol. 148, pp. 650–658, 2018.
- [25] Y.-H. Yu, N. Tom, and D. Jenne, "Numerical analysis on hydraulic power take-off for wave energy converter and power smoothing methods," in *ASME 2018 37th International Conference on Ocean, Offshore and Arctic Engineering*. American Society of Mechanical Engineers Digital Collection, 2018.
- [26] V. Piscopo, G. Benassai, L. Cozzolino, R. Della Morte, and A. Scamardella, "A new optimization procedure of heaving point absorber hydrodynamic performances," *Ocean Engineering*, vol. 116, pp. 242–259, 2016.
- [27] C. Lee, *WAMIT Theory Manual*, ser. Report (Massachusetts Institute of Technology. Department of Ocean Engineering). Massachusetts Institute of Technology, Department of Ocean Engineering, 1995. [Online]. Available: <http://books.google.com/books?id=fWKGHAAACAAJ>
- [28] T. Pérez and T. I. Fossen, "Time-vs. frequency-domain identi-

- fication of parametric radiation force models for marine structures at zero speed," *Modeling, Identification and Control*, vol. 29, no. 1, pp. 1–19, 2008.
- [29] J. Falnes, *Ocean Waves and Oscillating Systems - Linear Interactions Including Wave-Energy Extraction*. Cambridge University Press, 2002, ch. 4.
- [30] T. C. Austin, J. B. Edson, W. R. McGillis, M. Purcell, R. A. Pettit, M. K. McElroy, C. W. Grant, J. Ware, and S. K. Hurst, "A network-based telemetry architecture developed for the Martha's Vineyard coastal observatory," *IEEE Journal of Oceanic Engineering*, vol. 27, no. 2, pp. 228–234, 2002.
- [31] H. Jiang and G. Chen, "A global view on the swell and wind sea climate by the Jason-1 mission: a revisit," *Journal of Atmospheric and Oceanic Technology*, vol. 30, no. 8, pp. 1833–1841, 2013.
- [32] O. Abdelkhalik and S. Zou, "Time-varying linear quadratic gaussian optimal control for three-degree-of-freedom wave energy converters," in *European Wave and Tidal Energy Conference 2017*, 2018.